

## Post 4 Ma initiation of normal faulting in southern Tibet. Constraints from the Kung Co half graben

G. Mahéo<sup>a,\*</sup>, P.H. Leloup<sup>b</sup>, F. Valli<sup>c</sup>, R. Lacassin<sup>c</sup>, N. Arnaud<sup>d</sup>, J.-L. Paquette<sup>e</sup>,  
A. Fernandez<sup>b</sup>, L. Haibing<sup>f</sup>, K.A. Farley<sup>a</sup>, P. Tapponnier<sup>c</sup>

<sup>a</sup> Division of Geological and Planetary Sciences, California Institute of Technology, 1200E California Blvd, Pasadena CA91125, USA

<sup>b</sup> Université de Lyon, Université Claude Bernard Lyon1, Ecole Normale Supérieure de Lyon, Laboratoire de Sciences de la Terre,  
UMR 5570 CNRS, 2 rue Dubois, Bat géode, la Doua, 69622 Villeurbanne, France

<sup>c</sup> Institut de Physique du Globe de Paris, 4 place Jussieu, 75252 Paris CEDEX 05, France

<sup>d</sup> I S T E M - U S T L, Place Eugène Bataillon, 34095 Montpellier Cedex 5, France

<sup>e</sup> Laboratoire Magmas et Volcans, UMR 6524 CNRS, Université Blaise Pascal, rue Kessler, 63036 Clermont Ferrand, France

<sup>f</sup> Institute of Geology, Chinese Academy of Geological Sciences, 26 Baiwanzhuang Raod, Beijing 100037, PR China

Received 17 January 2006; received in revised form 23 January 2007; accepted 25 January 2007

Available online 2 February 2007

Editor: C.P. Jaupart

### Abstract

The timing of E–W extension of the Tibetan plateau provides a test of mechanical models of the geodynamic evolution of the India–Asia convergence zone. In this work we focus on the Kung Co half graben (Southern Tibet, China), bounded by an active N–S normal fault with a minimum vertical offset of 1600 m. To estimate the onset of normal faulting we combined high and medium temperature (U–Pb, Ar/Ar) and low temperature ((U–Th)/He) thermochronometry of the Kung Co pluton, a two-mica granite of the northern Himalayan granitic belt that outcrop in the footwall of the fault. Biotite and muscovite Ar/Ar ages, are close from each other [ $\sim 16 \text{ Ma} \pm 0.2 \text{ (Ms)}$  and  $\sim 15 \pm 0.4 \text{ Ma (Bt)}$ ], which is typical of fast cooling. The zircon and apatite (U–Th)/He ages range from 11.3 to 9.6 Ma and 9.9 to 3.7 Ma respectively. These He ages are indicative of (1) fast initial cooling, from 11.3 to  $\sim 9 \text{ Ma}$ , gradually decreasing with time and (2) a high geothermal gradient ( $\sim 400 \text{ }^\circ\text{C/km}$ ), close to the surface at  $\sim 10 \text{ Ma}$ .

The Kung Co pluton was emplaced at about 22 Ma (U–Pb on zircon) at less than 10 km depth and 520–545  $^\circ\text{C}$ . Subsequent to its shallow emplacement, the pluton underwent fast thermal re-equilibration ending around 7.5 Ma, followed by a period of slow cooling caused either by the end of the thermal re-equilibration or by very slow exhumation (0.02–0.03 mm/yr) from  $\sim 7.5 \text{ Ma}$  to at least 4 Ma. In either case the data suggest that the exhumation rate increased after 4 Ma. We infer this increase to be related to the initiation of the Kung Co normal fault. A critical examination of previously published data show that most  $\sim \text{N–S}$  Tibetan normal faults may have formed less than 5 Ma ago rather than in the Miocene as assumed by several authors. Such a young age implies that E–W extension is not related to the Neogene South Tibetan magmatism (25 to 8 Ma). Consequently, models relating E–W extension to magmatism, such as convective removal of the lower lithosphere, may be inappropriate. We rather think that this extension is related with local accommodation of boundary forces and displacements.

© 2007 Elsevier B.V. All rights reserved.

**Keywords:** Tibetan Plateau; normal fault; U–Pb; Ar/Ar and (U–Th)/He thermochronology; Pliocene activation

\* Corresponding author. Now at Université Claude Bernard Lyon1, 2 rue Dubois, Bat géode, la Doua, 69622 Villeurbanne, France. Tel.: +33 4 72 44 62 36; fax: +33 4 72 44 85 93.

E-mail address: [gweltaz.maheo@univ-lyon1.fr](mailto:gweltaz.maheo@univ-lyon1.fr) (G. Mahéo).

## 1. Introduction

In continental collision context, following an initial thickening episode, some orogenic domains undergo development of normal faults and extension in a still actively converging context. Perhaps, the most striking example of current orogenic extension is the southern Tibetan north of the Himalayas. The Tibet plateau is the largest active orogen, a direct result of the India–Asia collision. The most recent tectonic regime, especially south of the Bangong Nujiang suture is characterized by the occurrence of numerous active normal faults, with a roughly north–south orientation (Fig. 1A [1,6,7]). These faults result from east–west directed extension, perpendicular to India–Asia convergence. Two main groups of models have been proposed to explain this extension. The first one relates the extension to the dissipation of excess potential energy accumulated either during the thickening of the Asian margin or during the uplift of the plateau following detachment of the lithospheric part of the Asian plate (e.g. [8]). The second group of models links the extension to the local accommodation of boundary forces and displacements [2]. In this case, extension is related to locally oblique convergence between India and Asia [9], to the curvature or outward expansion of the Himalayan arc [1,10–12], or to the eastward extrusion of northern Tibet [13].

The initiation age of the normal faults is a key observation by which to discriminate between the models. Especially if timing of extension is contemporaneous with magmatic pulses models have to explain both events. Moreover it is crucial to determine if E–W extension occurs during a single event or if several phases can be recognized, thus raising the possibility of successive mechanism. Tectonic structures interpreted to result from E–W extension have different reported ages ranging from 18 to 8 Ma (e.g., [3,14–16]). This has led many authors to propose that E–W extension in southern Tibet started before 8 Ma. However, as we will see in discussion, such ages can be disputed as the dated faults (for instance in the Himalayas and Nyainqentangla range) may have undergone a more complex history than a simple E–W extension. The only age constraint specific to E–W extension in the south-Tibetan grabens is that proposed by Armijo et al. [1], who used regional

tectonic and stratigraphic arguments combined with quaternary normal faulting rates to suggest that extensional faulting *sensu stricto* started after 2.5 Ma. This estimate however is also questionable, as it rests on few stratigraphic constraints, and on the extrapolation of Quaternary fault rates based on qualitative inference of glacial moraines ages.

In this work we examine the time history of development of one of the most typical, west dipping normal fault bounding the Kung Co half graben located between the Indus Zangbo suture and the crest of the Himalayan range (Fig. 1, see also Fig. 3 in [1]). It has a minimum vertical offset of about 1600 m [1], and has exhumed a granite pluton in its footwall. Our goal is to reconstruct the thermal history of the Kung Co granite in order to obtain quantitative age bounds on the tectonic events that affected the area, including E–W extension that we infer to be responsible for its local exhumation. For this, we combined high (U–Pb), medium (Ar/Ar) and low temperature [(U–Th)/He] thermochronometric techniques to the mineral assemblages in the granite.

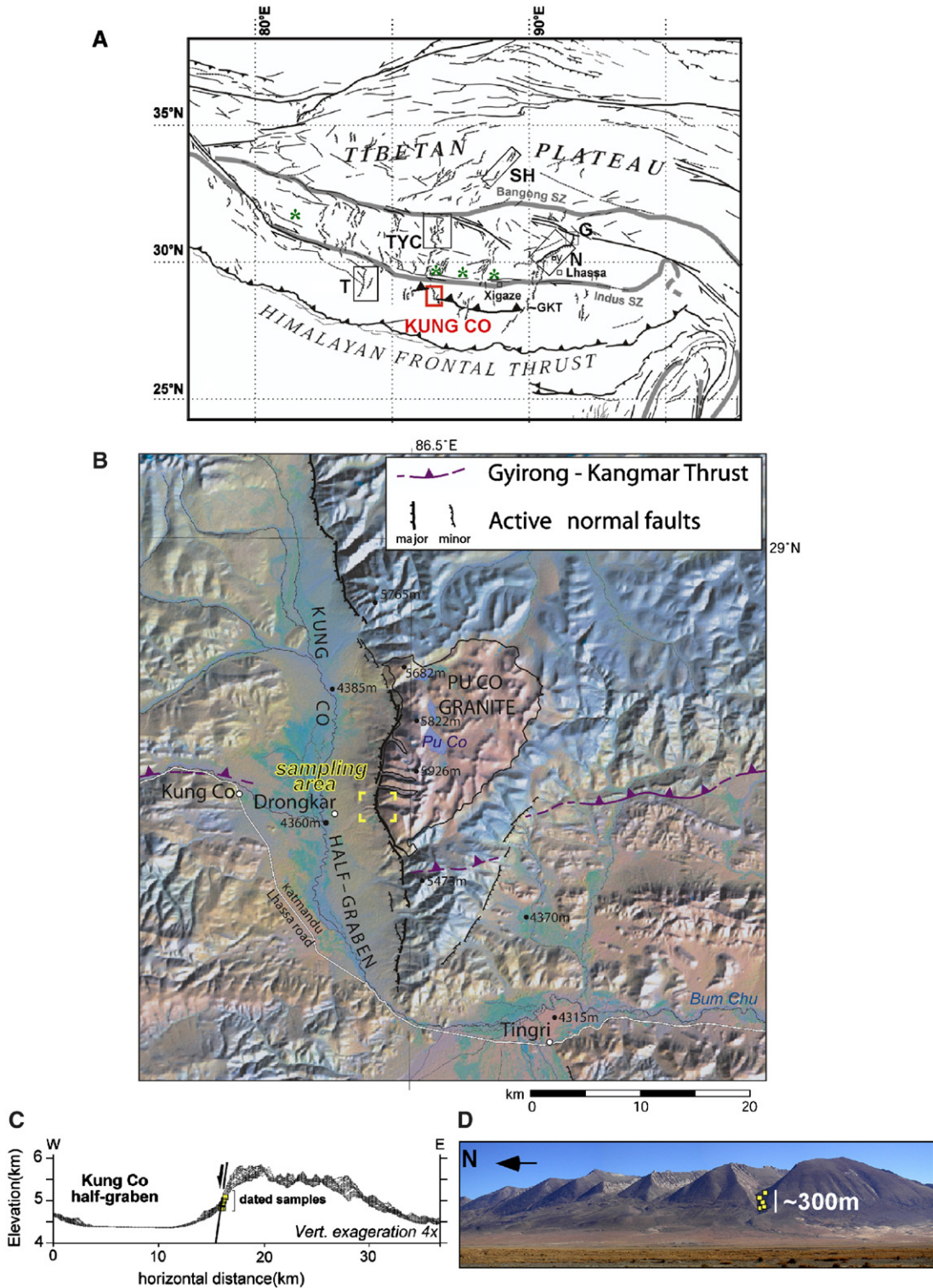
## 2. Structural and geological setting

The mountain front east of the flat Kung Co graben floor shows abundant evidence of rapid quaternary normal faulting: steep 800 m high triangular facets, hanging glacial valleys, as well as offset moraines and till deposits, (Fig. 1B, C and D) [1]. The fault plane, which is exposed at the base of the facets, is steep, dipping 50° to 60° W [1]. The active normal fault crosscuts the south Tibetan antiform [17,18], an crustal-scale ~E–W trending fold, that developed within the Tethys Himalayas thrust-stack during the Miocene above the Gyirong–Kangmar south-verging thrust (GKT, [5]). Mapping by Burg et al. [4] indicates that the GKT extends from Kangmar to the Kung Co area (Fig. 1A), where it is cut and offset by the half graben (Fig. 1B). The footwall of the normal fault bounding the Kung Co half graben consists of Cenozoic Tethyan sediments and metasediments intruded by the two-mica Kung Co or PuCo granite (Fig. 1B). This granite belongs to the north-Himalayan plutonic belt, whose emplacement ages span the period between 9.5 Ma and 27.5 Ma [19–21]. The granite is surrounded by a contact aureole of metasedimentary rocks characterized by the

Fig. 1. Structural setting of the Kung Co half graben and sample location. (A) Main active faults (black) and suture zones (grey) of the India–Asia collision zone (after [1,2]). Green \* N–S trending andesitic dykes from Williams et al. [3]. Trace of Gyirong–Kangmar thrust (GKT) from Burg et al. [4] and Lee et al. [5]. G: Gulu rift, N: Nyainqentangla graben, T: Thakkhola graben, TYC: Tangra Yum Co rift, SH: Shuang Hu graben, y: Yangbajing. (B) Landsat satellite image and Digital Elevation Model (SRTM data) of Kung Co area and main tectonic features (Gyirong–Kangmar Thrust location modified after Burg et al. [4]). (C) E–W topographic profiles across Kung Co half graben and normal fault (SRTM data) and sampling locations. (D) Photograph of Kung Co normal fault and sampling location. View towards the east from valley floor.

presence of andalusite+muscovite+biotite and late chlorite. Staurolite and biotite are observed as inclusions within the andalusite. The peak metamorphic conditions

recorded by the contact aureole, as modeled using the *Perple\_X* software [22], and internally consistent dataset for minerals and fluids of Holland and Powell [23] are



estimated to be 520–545 °C and less than 3 kbar. The peak metamorphic conditions recorded by the contact aureole are related with the depth and the temperature at which the pluton is intruded within the metasediments. These results indicate that the pluton was emplaced at a relatively shallow depth (less than 10 km), and was still relatively hot when intrusion stopped. Such observations imply that the intrusion took place from melt temperatures down to 520–545 °C, suggesting post-crystallization solid-state diapiric ascent as already suggested for northern Himalayan plutons by Le Fort [18].

### 3. Thermochronology, analytical methods and results

We collected 5 samples of the two-mica granite along an elevation transect in the footwall of the normal fault at altitudes between 4810 and 5080 m (Fig. 1C and D). The maximum vertical elevation difference between the samples is 270 m and the horizontal distance, 600 m. All samples were submitted to apatite and zircon (U–Th)/He dating, two samples for biotite Ar/Ar dating, and one for muscovite Ar/Ar dating. The two samples used for biotite Ar/Ar dating were also processed for zircon U–Pb dating (Table 1).

#### 3.1. U–Pb dating

The zircon fractions were dissolved and analyzed at the University of Clermont-Ferrand by ID-TIMS following the technique described by Paquette and Pin [24]. Each fraction (4 to 22 grains) was transferred into a Teflon microcapsule and then arranged in a 120-ml PTFE Teflon bomb enclosed in a stainless steel jacket following the method of Parrish [25]. The zircon fractions were spiked with  $^{205}\text{Pb}$ – $^{235}\text{U}$  and dissolved in HF at 220–230 °C for 20 h (see [24] for details). Prior to analysis, U and Pb were separated using micro-columns filled with TRU-Spec-SR. Spec mixed resins (see [24] for details). The samples were loaded on Re filaments with silica-gel and phosphoric acid. The Pb and  $\text{UO}_2$  isotope ratios were measured on a VG Sector 54-30 mass spectrometer. Pb isotope ratios were recorded in multicollector static mode (see [24] for details),  $^{204}\text{Pb}$  being simultaneously measured with a Daly detector ion-counting system. Analytical results are available in the electronic supplement (Table A1).

$^{206}\text{Pb}/^{238}\text{U}$  and  $^{207}\text{Pb}/^{235}\text{U}$  ratios have been plotted on a Concordia diagram (Fig. 2). The data define discordia lines with lower intercepts of  $22.0 \pm 2.7$  Ma and  $22.1 \pm 1.1$  Ma for samples K2L175 and K2P86 respectively. The corresponding upper intercepts are

$679 \pm 34$  and  $675 \pm 14$  Ma respectively. The intercepts of the two samples are identical within errors suggesting that they are robust even if calculated with few data points. We interpret the lower intercepts to date the Kung Co granite crystallization at  $22 \pm 2.7$  Ma. This age is in the 9.5–27.5 Ma range of previously published ages for the north-Himalayan granites [19–21].

#### 3.2. Ar/Ar dating

Whole rocks were crushed, sieved and individual grains selected using a high-power binocular microscope. All separates were irradiated in a single irradiation, at the MacMaster reactor (Ontario) in position 5C. The J-factor was estimated by the use of duplicates of the Fish Canyon sanidine standard with an age of 28.48 Ma [26,27] at a value of 0.01176 with 1% relative standard deviation. Interfering nuclear reactions on K and Ca were calculated by co-irradiation of pure salts. Samples were loaded in aluminum packets into an induction furnace where temperature is calibrated by means of an optical pyrometer, and step heated in classical fashion from 700 °C to 1400 °C. Each step lasted for 20 min. The gas was purified using cold traps with liquid air and Al–Zr getters. Once cleaned, the gas was introduced into a VG3600 mass spectrometer. Two minutes were allowed for equilibration before statistical analysis. Signals were measured by means of a Faraday cup with a resistor of  $10^{11}$  ohm for  $^{40}\text{Ar}$  and  $^{39}\text{Ar}$  while  $^{39}\text{Ar}$ ,  $^{38}\text{Ar}$ ,  $^{37}\text{Ar}$  and  $^{36}\text{Ar}$  were analyzed with a photomultiplier after interaction on a Daly plate. Gain between collectors was estimated by duplicate analysis of  $^{39}\text{Ar}$  during each analysis, and also by statistical analysis over a period of several years. The gain averaged 95 and is known to be better than 1.5%. This uncertainty is propagated through the age calculation, along with analytical errors on each signal and errors on the blank values. Analytical results are given in Table A2. More detailed analytical results are available from N.A. upon request.

Analyzed samples show flat Ar/Ar age spectra for more than 60% of the released gas, for both biotite and muscovite (Fig. 3). The highest elevation sample (K2L175) gives a biotite plateau age of  $15.2 \pm 0.2$  Ma (Fig. 3, Table A2), confirmed by an inverse isochron age of  $15.8 \pm 0.2$  Ma (Fig. A2; Tables A2 and A3). For K2P86 both muscovite and biotite age spectra fall short of the strict definition of plateau ages; weighted mean ages were calculated on contiguous steps at  $16.4 \pm 0.2$  Ma and  $14.8 \pm 0.2$  Ma for the muscovite and the biotite respectively (Fig. 3, Tables A2 and A3). The two biotites show ages within uncertainty of each other,

Table 1  
Summary of the obtained ages

Sample	Elevation (m)	U–Pb Zr (Ma)	Ar/Ar Ms (Ma)	Ar/Ar Bt (Ma)	He Zr (Ma)	He Ap (Ma)
K2L175	5080	22.0±2.7		15.2±0.2	11.3±0.7	9.9±1.1
K2L176	4990				10.9±0.9	9.2±0.3
K2P86	4900	22.1±1.1	16.4±0.2	14.8±0.2	10.8±0.3	7.5±0.8
K2L173	4810				9.7±0.5	4.5±0.5
K2L172	4810				9.6±0.1	3.7±0.3

Ap : Apatite, Bt: Biotite, Ms: Muscovite, Zr: Zircon.

even though they are separated by 180 m of elevation. The muscovite gives a slightly older age.

### 3.3. (U–Th)/He dating

The granites yielded small numbers of small to medium sized euhedral apatite and zircon grains (~70–195  $\mu\text{m}$  prism cross-section for apatite and ~60–140  $\mu\text{m}$  for zircon). For each sample 2 to 3 replicates of 1 to 3 apatites and 2 to 4 replicates of 2 to 4 zircons were dated. Analyzed grains were checked to be inclusions-free under a binocular microscope. Grain dimensions were measured under a microscope to determine the  $\alpha$  ejection correction [28]. All replicates were loaded in a platinum capsule and laser-heated for He extraction for 5 min at ~1050 °C (apatite) and 30 min at ~1300 °C (zircon) following the procedures described by House et al. [29] and Tagami et al. [30] respectively. Apatite capsules were transferred into Teflon beakers and dissolved and spiked with  $^{235}\text{U}$  and  $^{230}\text{Th}$ , and analysed on a Finnegan Element ICP-MS (see [29] for detailed analytical procedure). Zircon packets were transferred into graphite crucibles and fused with about 5 mg of ultra-pure  $\text{LiBO}_2$  at 1200 °C. After 1 h of heating, melted samples were instantaneously cooled to room temperature. The resulting glasses were then transferred into Teflon beakers with 1 ml of 10%  $\text{HNO}_3$ , spiked with  $^{235}\text{U}$  and  $^{230}\text{Th}$  and 4 ml of  $\text{H}_2\text{O}$ . These solutions were filtered to remove graphite particulates and analysed on a Finnegan Element ICP-MS.

For each sample we report the mean age of the replicates. For each replicate, typical analytical error on the age based on analytical uncertainty in U, Th and He measurement are 2% ( $1\sigma$ , [31]). However we report a 3% ( $1\sigma$ ) uncertainty for each individual sample based on the reproducibility of laboratory standards [31]. Uncertainties on the mean ages are reported as  $1\sigma$  standard errors using the standard deviation of the replicate analyses divided by  $(n-1)^{1/2}$  where n is the number of replicate analyses performed. This error estimate is larger than the analytical error alone and is intended to

reflect the age uncertainty due to differences in grain size, minor crystal defects, or zoning of parent material, which may contribute to grain differences in He age and uncertainties in the alpha-ejection correction (i.e. [32]). (U–Th)/He apatite and zircon analytical data are available in electronic supplement Table A4.

Apatite and zircon replicates gave relatively good reproducibility of (U–Th)/He measurements (the standard deviation represent less than 17% and 12% of the apatite and zircon age respectively). All ages are young, ranging between  $3.7\pm 0.3$  Ma and  $9.9\pm 1.1$  Ma for apatite and  $9.6\pm 0.1$  Ma and  $11.3\pm 0.7$  Ma for zircon (Fig. 4). The zircon ages correlate with elevation above sea level (Fig. 4), giving an apparent exhumation rate of ~0.15 mm/yr. The apatite ages obtained from the two highest samples give an apparent exhumation rate of ~0.15 mm/yr, similar to that obtained from the zircons, while the three lowest elevation samples (K2L172, 173 and K2P86) define a significantly different age–elevation relationship, with a lower apparent exhumation rate of ~0.03–0.02 mm/yr (Fig. 4).

## 4. Cooling and exhumation history of the Kung Co granite

To develop cooling histories we calculated Ar and He closure temperatures for cooling rates ranging from 1 °C/km to 100 °C/km following the method of Dodson [33], using diffusion parameters for Ar in muscovite [34] and biotite [35], as well as for He in zircon [36] and apatite [37]. The calculated closure temperatures are  $370\pm 35$  °C for Ar in muscovite,  $300\pm 30$  °C for Ar in biotite,  $180\pm 20$  °C for He in zircon and  $70\pm 15$  °C for He in apatite.

Samples K2P85 and K2L175 for which both Ar/Ar and (U–Th)/He ages have been obtained show very similar cooling histories (Fig. 5). The data suggest that, after the granite crystallized at ~22 Ma, cooling was fast (~80±20 °C/Ma from 22.0 to 16.5 Ma and 70±25 °C/Ma between 16.5 to 15.0 Ma, Table 1, Fig. 5). Fast cooling is also suggested by the almost identical biotite

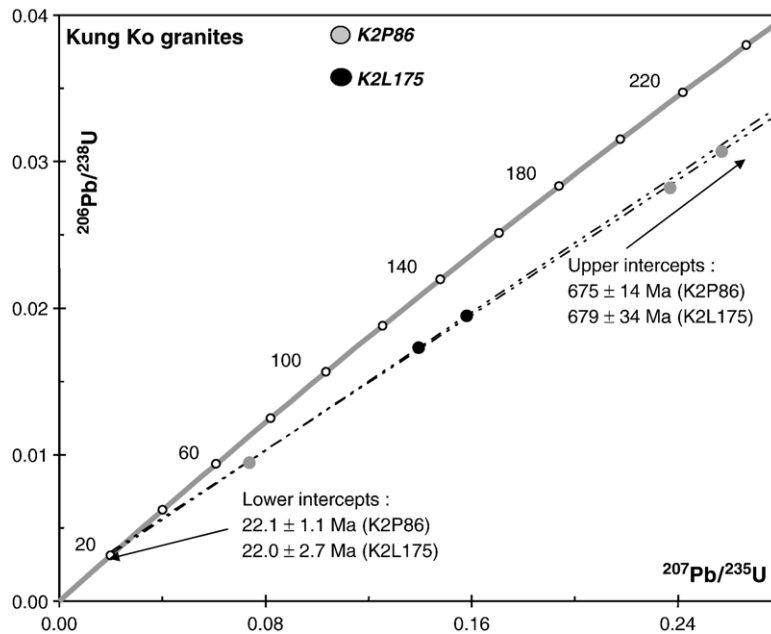


Fig. 2. Zircon U–Pb concordia diagram for samples K2P86 and K2L175 of Kung Co granite. Numbers on Concordia curve are ages in Ma. Intercepts are intersection points between Concordia curve and Discordia line defined by measured ratios.

Ar/Ar ages for the two samples separated by 180 m elevation, assuming vertical cooling. After  $\sim 15$  Ma and until  $\sim 7.5$  Ma the vertical cooling rate slowed but remained relatively high ( $>25$  °C/Ma, Table 1, Fig. 5). Actually, within error the apatite He age of the highest elevation sample (K2L175) is the same as all of the zircon He ages at  $\sim 10$  Ma (Fig. 4). The vertical distance between the lowest and the highest sample (270 m), thus provides the minimum vertical distance between the apatite and zircon (U–Th)/He isotherms ( $\sim 70$  °C and 180 °C respectively) at  $\sim 10$  Ma. This implies a minimum geothermal gradient of  $\sim 400$  °C/km at that time. This calculation assumes that the section has not been tilted after 10 Ma. If tilting occurred, the calculated geothermal gradient would be even greater. As the apatite and zircon He closure temperatures are relatively low, the calculated high geothermal gradient corresponds to shallow depths and could only be reached close to a shallow magmatic intrusion. This assertion is compatible, first, with the thermobarometric study of the contact aureole of the pluton that indicates that intrusion stopped at less than 10 km depth and when the pluton temperature was  $\sim 520$ – $545$  °C, and second with the rapid cooling evidence derived from Ar/Ar and U/Pb thermochronology previously discussed (Fig. 5). We thus consider that the time – temperature history recorded by the pluton from its crystallization at about 22 Ma until  $\sim 7.5$  Ma is related to diapiric intrusion

of the pluton and its subsequent post-intrusion thermal re-equilibration. As the temperature of the intrusion ( $\sim 520$ – $545$  °C) is higher than the closure temperature for Ar in both biotite and muscovite, the measured Ar/Ar ages of 15–16 Ma yield a minimum estimate for the age of intrusion. Based on the cooling history in Fig. 5, the age at which the pluton reached 520–545 °C can be estimated to be  $\sim 18$  Ma.

On the age–elevation plot (Fig. 4) the apparent exhumation rate given by the apatite He ages decreases progressively from  $\sim 0.15$  mm/yr (from 9.9 to 9.2 Ma) to 0.05 mm/yr (from 9.2 to 7.5 Ma) and 0.02–0.03 mm/yr (from 7.5 to 4 Ma). This gradual decrease can be associated with the end of the thermal relaxation.

If one then assumes that the apparent exhumation rate remained constant since 7.5 Ma, extrapolation of the age elevation relationship (Fig. 4) would yield the expected present-day depth at which apatite He ages would be zero (Fig. 4). This would correspond to the present-day position of the closure temperature isotherm for He diffusion in apatite. Using the Fig. 4 plot, the resulting elevation is  $\sim 4700$  m, only about 300 m below the mean local sampling elevation (Fig. 1C) and would imply a geothermal gradient of  $\sim 315$  °C/km close to the surface. Measurements of the present day surface heat flow in southern Tibet range between 60 and 100 mW/m<sup>2</sup> [38], implying a geothermal gradient

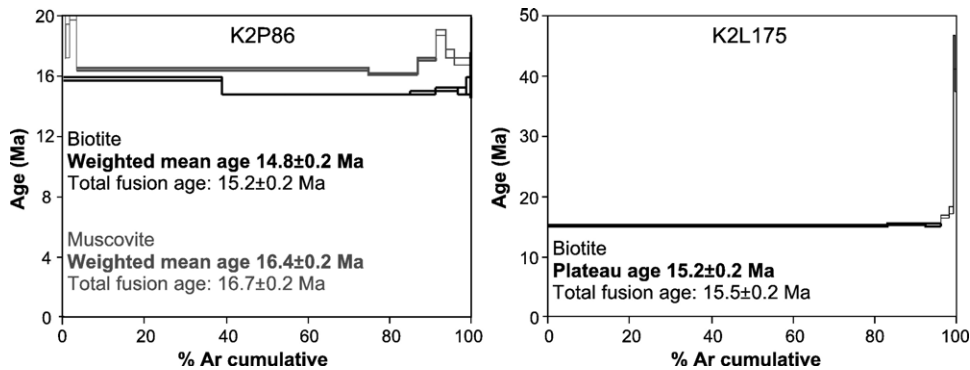


Fig. 3. K2P86 and K2L175 mica  $^{40}\text{Ar}/^{39}\text{Ar}$  age spectra. Steps used for simple mean weighted or plateau age calculation are shown in heavy line.

between  $\sim 40$  °C/km and  $\sim 23$  °C/km (for a thermal conductivity of  $2.5 \text{ W/m}^{-1}$ ). There is no field evidence, as hot spring or recent volcanics, for a locally higher heat flow in Kung Co. Present day geothermal gradient values are thus incompatible with the very high geothermal gradient obtained by assuming a constant apparent exhumation rate since 7.5 Ma.

Consequently we infer that the apparent exhumation rate changed between  $\sim 4$  Ma and the present day. In order to estimate the value of the mean apparent exhumation rate after 4 Ma, we determined the present day depth of the closure temperature for He in apatite. Based on the measured values of the geothermal gradient ( $\sim 40$  °C/km to  $\sim 23$  °C/km, [38]) the closure temperature for He diffusion in apatite should lie between 1.4 and 3.7 km below the surface. This implies that since  $\sim 4$  Ma the average exhumation rate has been between 0.35 and 0.93 mm/yr, ten times higher than that between 7.5 and 4 Ma (Fig. 6). Thus, an acceleration of the exhumation rate is required to explain the observed apatite He age–elevation relationship.

Alternatively, the young apatite He ages might be explained in two other ways: (1) by fluid assisted local heat advection, (2) by a fault raising the lowest samples with respect to the other ones. The youngest ages (3.7–4.5 Ma), however, have been obtained from two samples 10 m apart, and all samples are unaltered granites without mineralogical evidence for fluid circulation. Furthermore we have not observed evidence for metasomatism and fluid circulation at outcrop scale. We conclude that focussed heat advection is improbable. Similarly, there is no evidence in the field for an East dipping normal fault or a West dipping thrust that would have lifted up the lowest samples relative to the other samples. Moreover, such a fault would have also affected the zircon He age–elevation plot, which is clearly not the case (Fig. 4). We thus conclude that the youngest apatite He ages indicate that relatively fast exhumation started after  $\sim 4$  Ma.

The thermal/exhumation history of the Kung Co granite can be summarized as follows. The formation of the Kung Co granite took place at  $\sim 22$  Ma, and was followed by diapiric ascent up to a least 10 km and partial thermal re-equilibration to 520–545 °C before 16 Ma (Fig. 5). Shallow thermal re-equilibration and associated fast cooling lasted until  $\sim 7.5$  Ma. Then the pluton experienced slow cooling and slow exhumation of about 0.025 mm/yr from 7.5 to at least 4 Ma. Finally, fast exhumation started less than  $\sim 4$  Ma ago.

## 5. Discussion

### 5.1. Mechanisms for exhumation of the Kung Co pluton

The Kung–Co pluton experienced at least two significant episodes of cooling/exhumation (1) from its crystallisation at 22 Ma to the end of its intrusion at less than 10 km depth and 520–545 °C before 16 Ma and (2) after 4 Ma. The first episode is related to diapiric ascent

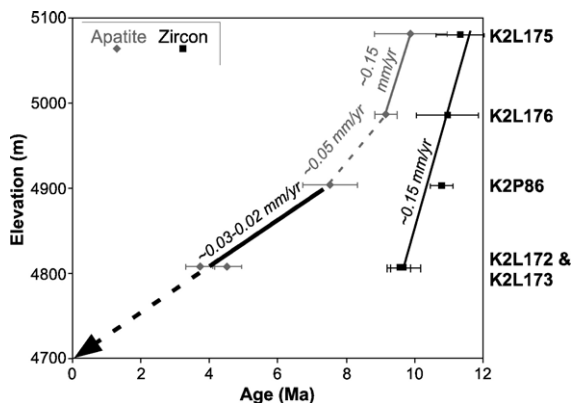


Fig. 4. Plot of apatite (diamond) and zircon (square) (U–Th)/He ages versus elevation.

of the pluton while the most recent episode (1.4 to 3.7 km of exhumation, Fig. 6) likely corresponds to normal faulting [1]. As previously discussed, from 16 Ma to 7.5 Ma the cooling history of the pluton is primarily related to post-intrusion thermal re-equilibration. In this context of fast cooling ( $>25$  °C/Ma), the potential effects of tectonic exhumation on the cooling rates (Fig. 5) as well as on the apparent exhumation rates estimated from the He data (Fig. 4) are difficult to quantify. Consequently, the occurrence of tectonic exhumation before 7.5 Ma, contemporaneous with the thermal re-equilibration, cannot be excluded by our thermochronological data. Two main tectonic structures might have been active before 7.5 Ma: the Kung Co normal fault and the Gyirong–Kangmar south-vergent thrust (GKT, Fig. 1A and B). Southward thrusting along the GKT is related to the formation of the north Himalayan anticline [5]. Based on Ar/Ar and apatite fission tracks ages, Lee et al. [5] proposed that the GKT was active at  $\sim 11$  Ma, and possibly from 15 until 5.5 Ma. As the Kung Co pluton is located just north of the GKT, within the north Himalayan anticline and hanging wall of the GKT (Fig. 1A and B), and cooled rapidly between 16 and 7.5 Ma, tectonic exhumation related to south-directed thrusting on this thrust during thermal re-equilibration is likely. Early exhumation along the Kung Co normal fault would imply two distinct phases of normal faulting. The first one would have occurred in a ductile to brittle–ductile regime whereas the last one, associated with the present-day active normal fault, would have taken place solely in the brittle part of the crust. In the field, we did not observe any normal shear zones consistent with an early exhumation phase, later reactivated or crosscut by brittle normal faults. According to mapping by Burg et al. [4], the Kung Co normal fault cuts and offsets the GKT (Fig. 1B). This indicates that the Kung Co normal fault formed after 11 Ma, or even after 5.5 Ma. Based on the relationship between the GKT and the Kung – Co normal fault, and on the lack of evidence for ductile normal shear, it is thus likely that the age of onset of the active Kung Co normal fault is constrained by that of the most recent rapid cooling event, after  $\sim 4$  Ma.

### 5.2. Age for the onset of E–W extension in Tibet

Our study constrains the onset of fairly rapid extensional exhumation on a  $\sim$ N–S striking normal fault affecting the accreted Indian crust in south central Tibet. In this area, E–W extension would be quite recent ( $\leq 4$  Ma), significantly younger than nearby volcanic dykes, and younger than few initiation ages inferred for

other Tibetan normal faults. Should these results on the Kung Co normal fault be considered an exception, or closer to actually dating the onset of E–W extension in South-central Tibet?

Only  $\sim 75$  km north of the Kung Co graben, N–S trending andesitic and dacitic dykes (green asterisks in Fig. 1A) have been dated between 13.5 and 21 Ma [3]. The ultra-potassic composition of some dykes indicates that they probably result from mantle partial melting. Their occurrence has been attributed to the onset of E–W extension related to lithospheric delamination [3]. However in South Tibet, N–S shortening was still prevalent at  $\sim 11$  Ma, and probably since 15 Ma, during the formation of the GKT [5]. The N–S strike of the dykes only indicates that the minimal horizontal stress axis ( $\sigma_{h_{\min}}$ ) was  $\sim$ E–W at the time of volcanism, but not that extension was the prevalent stress regime with the maximum principal stress,  $\sigma_1$ , vertical. As commonly observed, such dykes could have simply formed in an intermediate stress regime with  $\sigma_1$  horizontal  $\sim$ N–S and  $\sigma_2$  vertical. Thus, there is little reason to use the age of such dykes as firm evidence for the onset of EW extension in South central Tibet.

Other evidence for early E–W extension in Tibet come from the Thakkhola and Nyainqentangla grabens, respectively located in SW Tibet and central Tibet (Fig. 1A). The Thakkhola graben, which is bounded to the west by the Danzardzong active normal fault, is filled by Mio-Pliocene detrital deposits of the Tetang (11–9.6 Ma) and Thakkhola ( $<7$  Ma) formations [39]. The 14 Ma Ar/Ar age on muscovites from a N–S trending hydrothermal vein in the Marsyandi valley south of the Thakkhola [14] has led several authors to infer that E–W extension started in the middle Miocene. However, as for the dykes, the age of such veins, whose formation does not require a vertical maximum principal stress ( $\sigma_1$ ), cannot be used to unambiguously assess the onset of E–W extension. In the Thakkhola graben, only the Thakkhola deposits, younger than 7 Ma, are unambiguously coeval with normal faulting along the Danzardzong fault. The underlying Tetang deposits may be associated either with piggy-back deposition [1] or motion on the South Tibet detachment system (STDS) [39]. A much younger age has also been proposed for both the Tetang (Pliocene) and the Thakkhola (Pleistocene) formations [40,41]. Such ages would restrict the E–W extension episode to the last  $\sim 5$  Myr.

In the Nyainqentangla (NQTL) graben, footwall thermochronology reveals two rapid cooling phases at 8 and 4 Ma [16]. The oldest cooling phase was ascribed to the onset of normal faulting [16] but in this area, the recent faults have unusually complex map geometry.

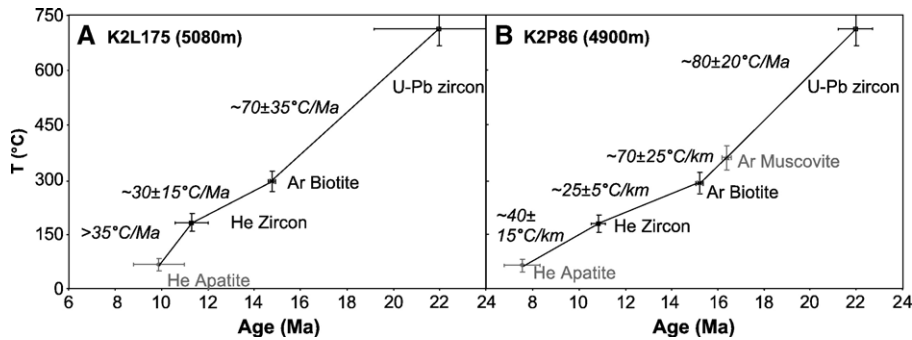


Fig. 5. Kung Co granite cooling history. A) K2L175. B) K2P86. Closure temperatures are:  $370\pm 35$  °C for Ar in muscovite;  $300\pm 30$  °C for Ar in biotite;  $180\pm 20$  °C for He in zircon and  $70\pm 15$  °C for He in apatite. For the U–Pb ages, crystallization temperature was inferred to be the same as for other North Himalayan pluton:  $720\pm 40$  °C after [21].

While they strike N–S west and south of Yangbajing, they veer to NE–SW along the NQTL range, parallel the NQTL ductile detachment [42] and the Damxung left lateral E–W shear zone [13], before veering back to N–S near Gulu [1] (Fig. 1). Our recent field mapping shows that the NQTL detachment is cut by the steeper normal faults and is absent west of Yangbajing and near Gulu. If, as Armijo et al. [13], we interpret the NE–SW striking stretch of active faults as a connection between

the two N–S grabens, guided by mechanical anisotropy resulting from previous structures, the formations of the NQTL ductile detachment and of the steep active faults may be considered as two independent events, possibly associated with the two distinct rapid cooling phases, at ( $\sim 8$  Ma) and (4 Ma), respectively. Moreover, using (U–Th)/He thermochronology, Stockli et al. [43], recently suggest that a major extension event occurs in the Gulu rift (Fig. 1), the northern prolongation of the NQTL, around 5–7 Ma.

In central Tibet, in the Tangra Yum Co rift, in the northern prolongation of the Kung Co Graben (Fig. 1), Dewane et al. [44] using (U–Th)/He thermochronometry recognized two episodes of exhumation. The first one started around 13 Ma and the second one at 6 Ma. They suggest that both events are related with E–W extension, but that the latest correspond with the more dominant pulses and is responsible for the modern rift topography [44].

In north central Tibet, in the Shuang Hu graben [45], the initiation age of normal faulting has been estimated to be older than 13.5 Ma. This age constraint is based on muscovite Rb/Sr and Ar/Ar total fusion ages from just one sample coming from a mineralized level following the graben-bounding normal fault. As along the NQTL, however, the west Shuang Hu fault trends NE–SW. Also, muscovites from the mineralized level are not deformed and show a perturbed Ar/Ar spectra. Moreover, muscovites within shear planes give a better age spectrum, with a weighted mean age of  $4\pm 0.2$  Ma. An alternative, more plausible, interpretation is thus that, while NE–SW faulting might have started prior to 13.5 Ma, E–W extension only started around 4 Ma, as in the Nyainqentangla.

Our thermochronological constraints, of the initiation of the Kung Co active normal fault after 4 Ma, together with the 4 Ma rapid cooling phase observed in the

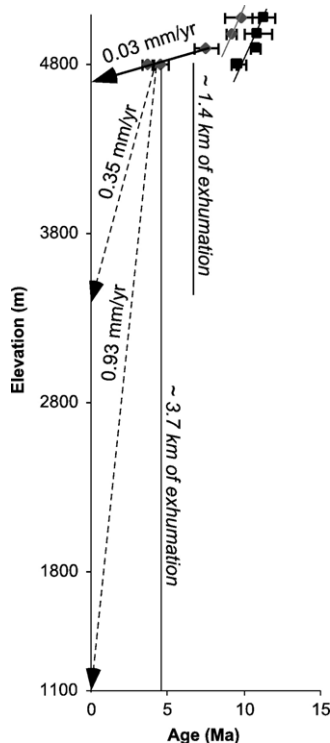


Fig. 6. Estimate of mean exhumation rate since 4 Ma. Bounds on the depths (1.4 km, 3.7 km) of present day closure temperature for He in apatite ( $55$  to  $85$  °C) are based on surface heat flow measured by Francheteau et al. [38].

Nyainqentangla, the possibly post 5 Ma faulting on the west side of the Thakkhola graben, and the extensional activation of the Shuang Hu graben at  $\sim 4$  Ma, suggest that widespread E–W extension in central and South Tibet might have started in the Pliocene, about 10 Ma later than thought by some authors [3,14–16], but not much before the onset date inferred by Armijo et al. (2.5 Ma [1]).

This new result has major implications for the structural evolution of the Tibetan plateau, and must be taken into account in tectonic models dealing with E–W extension. Such a young age would imply that E–W extension is not related to the Neogene South Tibetan magmatism, which spans the period from 25 to 8 Ma [46]. Consequently, models relating E–W extension with magmatism, such as convective removal of the lower lithosphere [3,8,45] would be inappropriate, and we rather think that this extension is related with local accommodation of boundary forces and displacements. Obviously, more data on the timing of E–W extension throughout Tibet are required to further constrain the age of extensional onset, assess whether it varies significantly, and better understand the triggering mechanism responsible for this peculiar “high-plateau” tectonic regime.

## Acknowledgments

This study was supported by the programs ‘Intérieur de la Terre’ (IT) and ‘Dynamique et Evolution de la Terre Interne’ (DYETI) of CNRS-INSU and by the Institute of Geology, Chinese academy of Geological Sciences, Beijing, China. Gweltaz Mahéo benefits from the Lavoisier Postdoctoral Fellowship. We thank Rolando Armijo and Stéphane Guillot for comments and discussion, and Lindsey Hedges and François Sénebier for their technical help.

## Appendix A. Supplementary data

Supplementary data associated with this article can be found, in the online version, at [doi:10.1016/j.epsl.2007.01.029](https://doi.org/10.1016/j.epsl.2007.01.029).

## References

- [1] R. Armijo, P. Tapponnier, J.L. Mercier, T. Han, Quaternary extension in Southern Tibet: field observations and tectonic implications, *J. Geophys. Res.* 91 (1986) 13803–13872.
- [2] P. Tapponnier, X. Zhiqin, F. Roger, B. Meyer, N. Arnaud, G. Wittlinger, Y. Jingsui, Oblique stepwise rise and growth of the Tibet plateau, *Science* 294 (2001) 1671–1677.
- [3] H. Williams, S. Turner, S. Kelley, N. Harris, Age and composition of dikes in Southern Tibet: new constraints on the timing of east–west extension and its relationship to postcollisional volcanism, *Geology* 29 (2001) 339–342.
- [4] J.P. Burg, A. Leyreloup, J. Girardeau, G.M. Chen, Structure and metamorphism of a tectonically thickened continental crust: the Yalu Tsangpo suture zone (Tibet), *Philos. Trans. R. Soc. Lond.* 321 (1987) 67–86.
- [5] J. Lee, B.R. Hacker, W.S. Dinklage, Y. Wang, P. Gans, A. Calvert, J.L. Wan, W.J. Chen, A.E. Blythe, W. McClelland, Evolution of the Kangmar Dome, southern Tibet: structural, petrologic, and thermochronologic constraints, *Tectonics* 19 (2000) 872–895.
- [6] P. Molnar, P. Tapponnier, Active tectonics of Tibet, *J. Geophys. Res.* 83 (1978) 5361–5375.
- [7] P. Tapponnier, J.L. Mercier, R. Armijo, T.L. Han, J. Zhou, Field evidence for active normal faulting in Tibet, *Nature* 294 (1981) 410–414.
- [8] P.C. England, G. Houseman, Extension during continental convergence, with application to the Tibetan Plateau, *J. Geophys. Res.* 94 (1989) 17561–17579.
- [9] R. McCaffrey, J. Nabelek, Role of oblique convergence in the active deformation of the Himalayas and southern Tibet Plateau, *Geology* 26 (1998) 691–694.
- [10] L. Seeber, J.G. Armbruster, Some elements of continental subduction along the Himalayan front, *Tectonophysics* 105 (1984) 263–278.
- [11] P. Molnar, H. Lyon-Caen, Fault plane solutions of earthquakes and active tectonics of the Tibetan Plateau and its margins, *Geophys. J. R. Astron. Soc.* 99 (1989) 123–153.
- [12] L. Seeber, A. Pêcher, Strain partitioning along the Himalayan arc and the Nanga–Parbat antiform, *Geology* 26 (1998) 791–794.
- [13] R. Armijo, P. Tapponnier, T. Han, Late Cenozoic right lateral strike–slip faulting in southern Tibet, *J. Geophys. Res.* 42 (1989) 11236–11268.
- [14] M. Coleman, K. Hodges, Evidence for Tibetan Plateau Uplift before 14-Myr Ago from a New Minimum Age for East–West Extension, *Nature* 374 (1995) 49–52.
- [15] C.N. Garzione, D. Dettman, J. Quade, P.G. DeCelles, R.F. Butler, High times on the Tibetan Plateau; paleoelevation of the Thakkhola Graben, Nepal, *Geology* 28 (2000) 339–342.
- [16] T.M. Harrison, P. Copeland, W.S.F. Kidd, O.M. Lovera, Activation of the Nyainqentangla Shear Zone: implications for uplift of the southern Tibetan Plateau, *Tectonics* 14 (1995) 658–676.
- [17] F. Debon, J.L. Zimmerman, J.H. Liu, C.W. Jin, R.H. Xu, Time relationships between magmatism, tectonics and metamorphism in three plutonic belts in southern Tibet: new K–Ar data, *Geol. Rundsch.* 74 (1985) 229–236.
- [18] P. Le Fort, Metamorphism and magmatism during the Himalayan collision, in: M.P. Cowards, A.C. Ries (Eds.), *Collision Tectonics*, *Geol. Soc. Spec. Publ.*, vol. 19, 1986, pp. 159–172.
- [19] U. Schärer, R.H. XU, C.J. Allègre, U–Th–Pb systematics and age of Himalayan leucogranites, South Tibet, *Earth Planet. Sci. Lett.* 77 (1986) 35–48.
- [20] T.M. Harrison, O. Lovera, M. Grove, New insights into the origin of two contrasting Himalayan granite belts, *Geology* 25 (1997) 899–902.
- [21] H.F. Zhang, N. Harris, R. Parrish, S. Kelley, L. Zhang, N. Rogers, T. Argles, J. King, Causes and consequences of protracted melting of the mid-crust exposed in the North Himalayan antiform, *Earth Planet. Sci. Lett.* 228 (2004) 195–212.
- [22] J.A.D. Connolly, Multivariable Phase-Diagrams— an Algorithm Based on Generalized Thermodynamics, *Am. J. Sci.* 290 (1990) 666–718.

- [23] T. Holland, R. Powell, Calculation of phase relations involving haplogranitic melts using an internally consistent thermodynamic dataset, *J. Petrol.* 42 (2001) 673–683.
- [24] J.L. Paquette, C. Pin, A new miniaturized extraction chromatography method for precise U–Pb zircon geochronology, *Chem. Geol.* 176 (2001) 311–319.
- [25] R.R. Parrish, An improved micro-capsule for zircon dissolution in U–Pb geochronology, *Chem. Geol.* 66 (1987) 99–102.
- [26] M.D. Schmitz, S.A. Bowring, U–Pb zircon and titanite systematics of the Fish Canyon Tuff: an assessment of high-precision U–Pb geochronology and its application to young volcanic rocks, *Geochim. Coschim. Acta* 65 (2001) 2571–2587.
- [27] M.D. Schmitz, S.A. Bowring, K.R. Ludwig, P.R. Renne, Comment on “Precise K–Ar, Ar-40–Ar-39, Rb–Sr and U–Pb mineral ages from the 27.5 Ma Fish Canyon Tuff reference standard” by M.A. Lanphere and H. Baadsgaard, *Chem. Geol.* 199 (2003) 277–280.
- [28] K.A. Farley, R.A. Wolf, L.T. Silver, The effects of long alpha-stopping distances on (U–Th)/He ages, *Geochim. Coschim. Acta* 60 (1996) 4223–4229.
- [29] M.A. House, K.A. Farley, D. Stockli, Helium chronometry of apatite and titanite using Nd-YAG laser heating, *Earth Planet. Sci. Lett.* 183 (2000) 365–368.
- [30] T. Tagami, K.A. Farley, D.F. Stockli, (U–Th)/He geochronology of single zircon grains of known Tertiary eruption age, *Earth Planet. Sci. Lett.* 207 (2003) 57–67.
- [31] K.A. Farley, (U–Th)/He dating: techniques, calibrations, and applications, in: D.P. Porcelli, C.J. Ballentine, R. Wieler (Eds.), *Noble Gases, Review in Mineralogy and Geochemistry*, vol. 47, 2002, pp. 559–577.
- [32] M.A. House, B.P. Wernicke, K.A. Farley, Paleo-geomorphology of the Sierra Nevada, California, from (U–Th)/He ages in apatite, *Am. J. Sci.* 301 (2001) 77–102.
- [33] M.H. Dodson, Closure temperature in cooling geochronological and petrological systems, *Contrib. Mineral. Petrol.* 40 (1973) 259–274.
- [34] W.E. Hames, S.A. Bowring, An empirical-evaluation of the argon diffusion geometry in muscovite, *Earth Planet. Sci. Lett.* 124 (1994) 161–167.
- [35] T.M. Harrison, I. Duncan, I. Mc Dougall, Diffusion of  $^{40}\text{Ar}$  in biotite: temperature, pressure, and compositional effects, *Geochim. Coschim. Acta* 44 (1985) 1985–2003.
- [36] P.W. Reiners, T.L. Spell, S. Nicolescu, K.A. Zanetti, Zircon (U–Th)/He thermochronometry: He diffusion and comparisons with Ar-40/Ar-39 dating, *Geochim. Coschim. Acta* 68 (2004) 1857–1887.
- [37] K.A. Farley, Helium diffusion from apatite: general behavior as illustrated by Durango fluorapatite, *J. Geophys. Res.* 105 (2000) 2903–2914.
- [38] J. Francheteau, C. Jaupart, X.J. Shen, W.H. Kang, D.L. Lee, J.C. Bai, H.P. Wei, H.Y. Deng, High heat-flow in southern Tibet, *Nature* 307 (1984) 32–36.
- [39] C.N. Garzzone, P.G. DeCelles, D.G. Hodkinson, T.P. Ojha, B.N. Upreti, East–west extension and Miocene environmental change in the southern Tibetan plateau: Thakkhola graben, central Nepal, *Geol. Soc. Amer. Bull.* 115 (2003) 3–20.
- [40] M. Colchen, The Thakkhola–Mustang graben in Nepal and the late Cenozoic extension in the Higher Himalayas, *J. Asian Earth Sci.* 17 (1999) 683–702.
- [41] M. Fort, Evolution geomorphologique d’une chaîne de collision intracontinentale: l’Himalaya central, transversale des Annapurnas, These d’Etat, Univ. Paris VII, 1993.
- [42] Y. Pan, W.S.F. Kidd, Nyainqentanghla shear zone — a Late Miocene extensional detachment in the Southern Tibetan Plateau, *Geology* 20 (1992) 775–778.
- [43] D. Stockli, M. Taylor, A. Yin, T.M. Harrison, J. D’Andrea, P. Kapp, L. Ding, Late Miocene–Pliocene inception of E–W extension in Tibet as evidenced by apatite (U–Th)/He data, *GSA Meet.* 34 (2002) 411.
- [44] T.J. Dewane, D.F. Stockli, C. Hager, M. Taylor, L. Ding, J. Lee, S. Wallis, Timing of Cenozoic E–W Extension in the Tangra Yum Co–Kung Co Rift, South-Central Tibet, AGU fall Meeting, 2006.
- [45] P.M. Blisniuk, B.R. Hacker, J. Glodny, L. Ratschbacher, B. Siwen, W. Zhenhun, M.O. McWilliams, A. Calvert, Normal faulting in central Tibet since at least 13.5 Myr ago, *Nature* 412 (2001) 628–632.
- [46] S.L. Chung, M.F. Chu, Y.Q. Zhang, Y.W. Xie, C.H. Lo, T.Y. Lee, C.Y. Lan, X.H. Li, Q. Zhang, Y.Z. Wang, Tibetan tectonic evolution inferred from spatial and temporal variations in post-collisional magmatism, *Earth-Sci. Rev.* 68 (2005) 173–196.

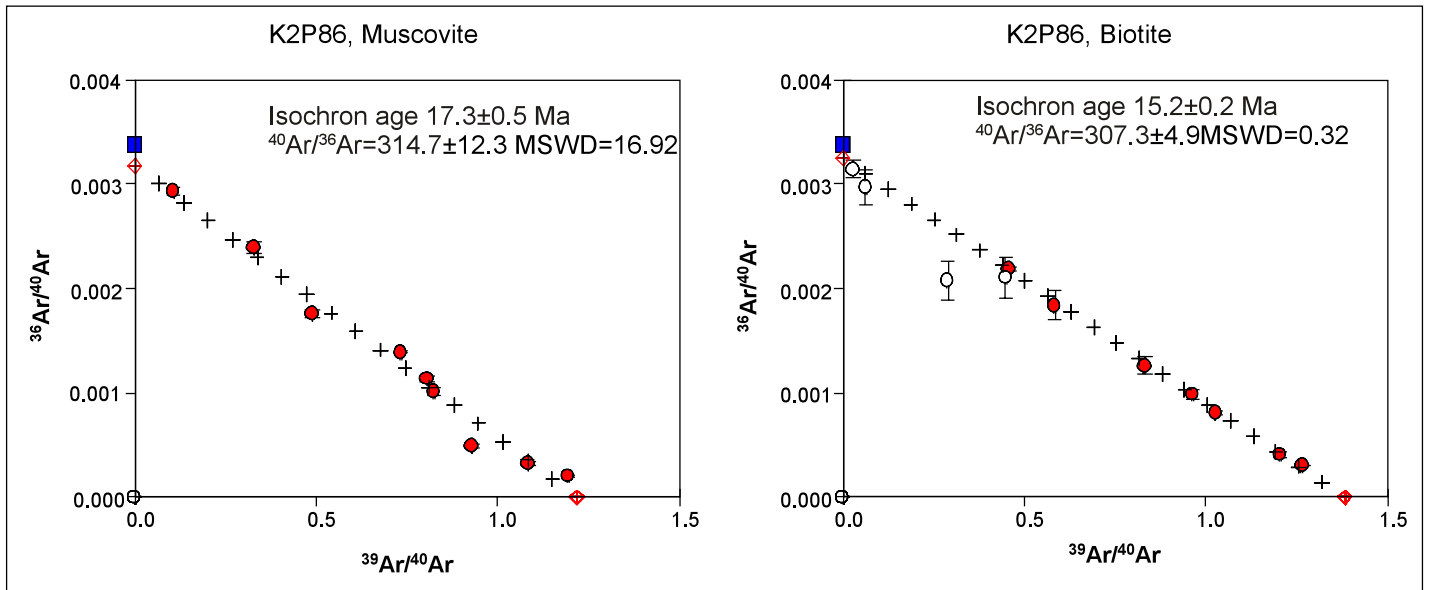


Fig. A1. Sample K2P86  $^{40}\text{Ar}/^{39}\text{Ar}$  isochrons from micas. Steps which were kept in the calculation are shown as red circles, those excluded as white circles. The  $^{36}\text{Ar}/^{40}\text{Ar}$  intercept is shown as a red open diamond and the air ratio as a blue square. The isochron ages are obtained in an inverse isochron diagram of  $^{36}\text{Ar}/^{40}\text{Ar}$  versus  $^{39}\text{Ar}/^{40}\text{Ar}$  [1] which allows homogeneous excess components to be individualized in many occasions. Errors on age and intercept are including individual errors on each point and linear regression by York's method [2]. The goodness of it relative to individual errors is measured with the Mean Square Weighted Deviation (MSWD).

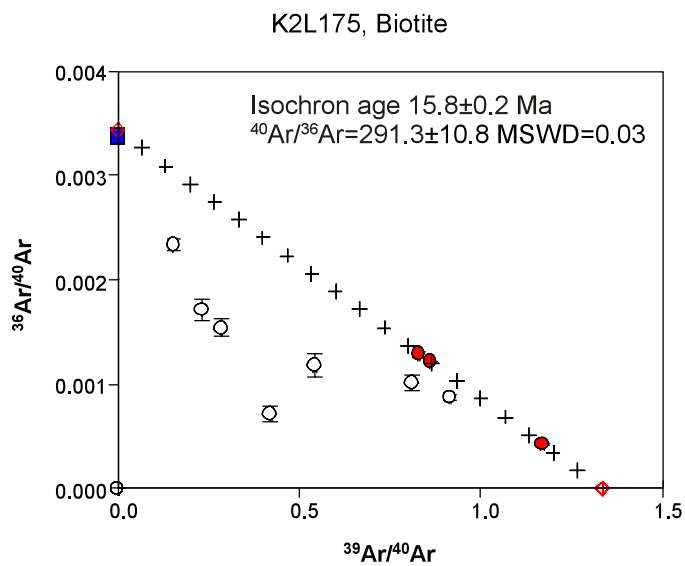


Fig. A2. Sample K2L175  $^{40}\text{Ar}/^{39}\text{Ar}$  spectra from biotite. Same symbols as Fig. A1.

Table A1  
U-Pb zircon analytical results

n°	Fraction	Wt (mg)	Concentration (ppm)		Atomic ratios					Apparent ages (Ma)			Correl coef
			U	Rad Pb	<sup>206</sup> Pb/ <sup>204</sup> Pb	<sup>208</sup> Pb/ <sup>206</sup> Pb	<sup>206</sup> Pb/ <sup>238</sup> U	<sup>207</sup> Pb/ <sup>235</sup> U	<sup>207</sup> Pb/ <sup>238</sup> U	<sup>206</sup> Pb/ <sup>235</sup> U	<sup>207</sup> Pb/ <sup>235</sup> U	<sup>207</sup> Pb/ <sup>238</sup> U	
<b>K2P86</b>													
1	[18] need.cl.un.	0.086	3,033	28.7	4909	0.1034	0.00945 ± 3	0.0738 ± 2	0.05669 ± 3	60.6	72.3	480	0.98
2	[4] sh.ly.un.	0.085	1,814	50.7	4914	0.0909	0.02821 ± 25	0.2370 ± 21	0.06094 ± 9	179	216	637	0.99
3	[4] lp.ly.un.	0.037	1,100	34.6	2006	0.1332	0.03069 ± 13	0.2570 ± 17	0.06074 ± 30	195	232	630	0.66
<b>K2L175</b>													
4	[22] need.cl.un.	0.127	2,165	40.4	10639	0.0520	0.01947 ± 8	0.1580 ± 6	0.05886 ± 3	124	149	562	0.99
5	[19] need.cl.un.	0.098	2,007	34.1	8943	0.0828	0.01729 ± 11	0.1395 ± 9	0.05853 ± 3	110	133	550	0.99

Individual analyses were performed on the least magnetic ( 2° forward and side tilt at 2.2 A using a Frantz Isodynamic magnetic barrier separator ) crack-free zircon grains. The isotopic ratios are corrected for mass discrimination ( 0.1 ± 0.015 % per amu for Pb and U ), isotopic tracer contribution and analytical blanks: 10 pg for Pb and less than 1 pg for U. Initial common Pb is determined for each fraction in using the Stacey & Kramers [3] two-step model. Absolute errors corresponding to the last significant digits are given at the 2σ level. Number in brackets is number of grains in fraction. Abbreviations: rad = radiogenic; need. = needle shaped; cl. = colourless; ly. = light yellow; un.= unabraded; sh. = short prismatic; lp. = long prismatic.

Table A2: Results of  $^{40}\text{Ar}/^{39}\text{Ar}$  Dating by Step Heating Analysis

Temp °C	$^{40}\text{Ar}/^{39}\text{Ar}$	$^{38}\text{Ar}/^{39}\text{Ar}$	$^{37}\text{Ar}/^{39}\text{Ar}$	$^{36}\text{Ar}/^{39}\text{Ar}$ ( $10^{-3}$ )	$^{39}\text{Ar}$ ( $10^{-4}$ moles)	$\text{F}^{39}\text{Ar}$ released	% $^{40}\text{Ar}^*$	$^{40}\text{Ar}^*/^{39}\text{Ar}$	Age Ma	$\pm 1\sigma$ Ma
K2P86		Muscovite		J= 0.011685						
700	9.287	0.030	0.002	27.285	0.13	0.69	12.97	1.20	25.21	2.00
800	3.048	0.013	0.002	7.296	0.20	1.70	28.62	0.87	18.30	1.11
900	2.042	0.012	0.001	3.583	0.36	3.51	47.17	0.96	20.19	0.51
950	1.364	0.009	0.000	1.899	13.98	74.82	57.40	0.78	16.43	0.09
1000	0.837	0.009	0.000	0.170	2.32	86.64	91.61	0.77	16.10	0.06
1050	0.923	0.010	0.000	0.301	0.93	91.36	88.20	0.81	17.07	0.10
1100	1.077	0.010	0.000	0.530	0.45	93.63	83.60	0.90	18.88	0.18
1200	1.216	0.011	0.000	1.232	0.42	95.75	68.40	0.83	17.44	0.30
1400	1.242	0.010	0.000	1.406	0.83	100.00	64.95	0.81	16.93	0.21
K2P86		Biotite		J= 0.011685						
500	2.189	0.014	0.000	4.792	13.00	38.80	34.39	0.75	15.80	0.17
600	0.791	0.012	0.000	0.239	15.41	84.80	88.56	0.70	14.71	0.04
700	0.831	0.013	0.000	0.340	2.11	91.11	85.49	0.71	14.91	0.12
800	0.975	0.012	0.000	0.793	1.74	96.31	73.91	0.72	15.12	0.13
850	1.037	0.012	0.000	1.022	0.75	98.54	68.94	0.72	15.01	0.31
900	1.204	0.013	0.001	1.521	0.28	99.37	61.03	0.73	15.43	0.60
950	1.711	0.013	0.003	3.147	0.10	99.65	44.50	0.76	15.98	1.47
1000	2.228	0.012	0.003	4.689	0.05	99.81	36.92	0.82	17.25	2.65
1100	3.452	0.014	0.004	7.187	0.04	99.92	37.91	1.31	27.38	3.92
1200	15.799	0.021	0.001	46.811	0.01	99.95	12.32	1.95	40.57	16.07
1400	33.558	0.028	0.000	105.360	0.02	100.00	7.16	2.40	49.98	16.68
K1L175		Biotite		J= 0.011685						
600	1.160	0.012	0.000	1.412	26.64	82.99	62.31	0.72	15.18	0.08
700	0.856	0.011	0.000	0.363	2.96	92.22	85.13	0.73	15.30	0.10
800	1.205	0.012	0.000	1.557	1.30	96.25	60.17	0.72	15.22	0.24
850	1.094	0.011	0.000	0.958	0.66	98.30	72.30	0.79	16.60	0.24
900	1.236	0.012	0.000	1.248	0.23	99.01	68.55	0.85	17.77	0.58
950	1.843	0.011	0.001	2.178	0.05	99.16	64.01	1.18	24.71	1.34
1000	2.378	0.011	0.001	1.706	0.04	99.29	77.97	1.85	38.67	1.17
1100	4.302	0.013	0.002	7.353	0.05	99.44	49.03	2.11	43.93	2.76
1200	3.481	0.011	0.000	5.359	0.09	99.72	53.94	1.88	39.15	1.84
1400	6.516	0.013	0.001	15.209	0.09	100.00	30.72	2.00	41.71	2.49

$^{40}\text{Ar}^*$  is defined as total  $^{40}\text{Ar}$  minus total atmospheric  $^{36}\text{Ar} \times 295.5$ , following the usual convention

Table A3: Summarized of  $^{40}\text{Ar}/^{39}\text{Ar}$  results

Sample	Elevation (m)	Mineral	Total fusion age (Ma)	Plateau (*) or weight mean age (Ma)	Inverse isochrone age (Ma)	Initial $^{40}\text{Ar}/^{36}\text{Ar}$
K2L175	5080	Bt	$15.5 \pm 0.2$	$15.2 \pm 0.2$ * Steps 1 to 3	$15.8 \pm 0.2$ Steps 1 to 3	$291.3 \pm 10.8$
K2P86	4900	Bt	$15.2 \pm 0.2$	$14.8 \pm 0.2$ Steps 1 to 7	$15.2 \pm 0.2$ Steps 1 to 7	$307.3 \pm 4.9$
K2P86	4900	Ms	$16.7 \pm 0.2$	$16.4 \pm 0.2$ Steps 3 to 5	$17.3 \pm 0.5$ All steps	$314.7 \pm 12.3$

Bt: Biotite, Ms: Muscovite

Table A4  
(U-Th)/He apatite analytical results

Sample	Elev. (m)	rep.	n	mass (mg)	He (ng/mol)	U (ppm)	Th (ppm)	radius ( $\mu\text{m}$ )	Ft	Raw age (Ma)	Corrected age (Ma)	1 $\sigma$ (Ma)
K2L172	4808	A	2	14.7	0.45	25.3	21.4	80.0	0.81	2.7	3.4	0.1
		B	3	4.5	0.86	43.7	47.8	38.1	0.66	2.9	4.4	0.1
		C	1	7.8	0.25	14.0	17.3	68.6	0.80	2.5	3.1	0.1
		D	1	1.9	0.60	32.0	31.9	40.0	0.68	2.8	4.1	0.1
		<b>mean</b>									<b>3.7</b>	<b>0.3</b>
K2L173	4808	A	1	5.4	1.71	47.9	200.3	54.3	0.75	3.3	4.4	0.1
		B	3	3.3	0.87	32.1	65.0	35.7	0.64	3.4	5.3	0.2
		C	1	8.0	1.75	78.2	129.1	62.8	0.79	3.0	3.8	0.1
		<b>mean</b>									<b>4.5</b>	<b>0.5</b>
K2P86	4904	A	3	19.3	1.91	52.8	3.3	74.3	0.80	6.6	8.2	0.2
		B	3	9.5	2.10	60.4	1.9	60.0	0.77	6.3	8.2	0.2
		C	1	1.5	2.14	58.9	161.1	40.0	0.66	4.1	6.2	0.2
		<b>mean</b>									<b>7.5</b>	<b>0.8</b>
K2L176	4987	A	2	21.0	1.98	45.8	4.4	85.7	0.83	7.8	9.4	0.3
		B	1	7.5	1.36	34.1	2.7	71.4	0.81	7.2	8.9	0.3
		<b>mean</b>									<b>9.2</b>	<b>0.3</b>
K2L175	5082	A	2	3.4	2.02	44.5	93.5	37.1	0.66	5.6	8.5	0.3
		B	2	12.3	2.43	57.7	3.9	65.7	0.79	7.6	9.6	0.3
		C	1	13.0	1.19	21.3	4.9	97.1	0.84	9.7	11.5	0.3
		<b>mean</b>									<b>9.9</b>	<b>1.1</b>

n: number of grains used, for each replicate 1 $\sigma$  is the analytical error, for the mean age the error is taken as the standard deviation divided by  $(n-1)^{1/2}$  where n is the number of replicates.

Table A5  
(U-Th)/He zircon analytical results

Sample	elev.	rep.	n	mass	He	U	Th	radius	Ft	raw age	corrected age	1 $\sigma$
	(m)			(mg)	(ng/mol)	(ppm)	(ppm)	( $\mu$ m)		(Ma)	(Ma)	(Ma)
K2L172	4808	A	3	9.1	81.5	2206	109.0	30.5	0.70	6.7	9.6	0.3
		B	3	19.1	56.7	1409	118.0	41.4	0.77	7.3	9.5	0.3
		<b>mean</b>										<b>9.6</b>
K2L173	4808	A	4	34.9	54.0	1214	132.0	48.9	0.79	8.0	10.0	0.3
		B	4	53.0	13.0	321	33.0	40.0	0.80	7.3	9.3	0.3
		<b>mean</b>										<b>9.7</b>
K2P86	4904	A	3	51.5	29.8	626	50.2	53.6	0.81	8.6	10.6	0.3
		B	3	66.7	53.3	1006	63.4	54.3	0.83	9.6	11.6	0.3
		C	4	43.8	52.7	1101	96.9	54.3	0.82	8.6	10.5	0.3
		D	2	37.9	43.5	845	147.8	61.4	0.83	9.1	10.9	0.3
		E	4	26.8	53.5	1130	70.6	38.9	0.76	8.6	11.3	0.3
		F	4	26.2	65.7	1601	106.1	38.6	0.76	7.4	9.8	0.3
<b>mean</b>										<b>10.8</b>	<b>0.3</b>	
K2L176	4987	A	2	59.5	33.0	653	81.0	71.4	0.86	9.1	10.6	0.3
		B	3	57.8	76.8	1318	219.9	62.4	0.84	9.0	12.3	0.4
		C	3	66.0	40.5	881	87.8	68.6	0.85	8.3	9.8	0.3
<b>mean</b>										<b>10.9</b>	<b>0.9</b>	
K2L175	5082	A	4	34.6	51.2	1115	78.0	42.1	0.79	8.3	10.7	0.3
		B	4	86.3	87.3	1425	93.8	58.2	0.84	11.1	13.2	0.4
		C	4	103.0	38.8	757	97.5	60.4	0.84	9.2	10.9	0.3
		D	3	35.4	43.3	924	88.5	46.7	0.80	8.4	10.5	0.3
<b>mean</b>										<b>11.3</b>	<b>0.7</b>	

n: number of grains used, for each replicate 1 $\sigma$  is the analytical error, for the mean age the error is taken as the standard deviation divided by  $(n-1)^{1/2}$  where n is the number of replicates.

- [1] J.C. Roddick, the application of isochron diagrams in  $^{40}\text{Ar}$ - $^{39}\text{Ar}$  dating: a discussion, Earth and Planetary Science Letters 48, 185-208, 1978.
- [2] D. York, Least Squares Fitting of a Straight Line with Correlated Errors, Earth and Planetary Science Letters 5(5), 320-324, 1969.
- [3] J.S. Stacey and J.D. Kramers, Approximation of Terrestrial Lead Isotope Evolution by a 2-Stage Model, Earth and Planetary Science Letters 26(2), 207-221, 1975.